

Biomechanics of Forearm Rotation: Force and Efficiency of Pronator Teres

Pere Ibáñez-Gimeno¹, Ignasi Galtés^{2,3}, Xavier Jordana⁴, Assumpció Malgosa¹, Joan Manyosa^{5*}

1 Unitat d'Antropologia Biològica, Departament de Biologia Animal, Biologia Vegetal i Ecologia, Universitat Autònoma de Barcelona, Bellaterra, Barcelona, Catalonia, Spain, **2** Centre de Patologia Forense de Collserola, Institut de Medicina Legal de Catalunya, Montcada i Reixach, Barcelona, Catalonia, Spain, **3** Unitat de Medicina Legal i Forense, Departament de Psiquiatria i de Medicina Legal, Universitat Autònoma de Barcelona, Bellaterra, Barcelona, Catalonia, Spain, **4** Departament de Paleobiologia, Institut Català de Paleontologia Miquel Crusafont (ICP), Universitat Autònoma de Barcelona, Bellaterra, Barcelona, Catalonia, Spain, **5** Unitat de Biofísica, Departament de Bioquímica i de Biologia Molecular, and Centre d'Estudis en Biofísica, Universitat Autònoma de Barcelona, Bellaterra, Barcelona, Catalonia, Spain

Abstract

Biomechanical models are useful to assess the effect of muscular forces on bone structure. Using skeletal remains, we analyze pronator teres rotational efficiency and its force components throughout the entire flexion-extension and pronation-supination ranges by means of a new biomechanical model and 3D imaging techniques, and we explore the relationship between these parameters and skeletal structure. The results show that maximal efficiency is the highest in full elbow flexion and is close to forearm neutral position for each elbow angle. The vertical component of pronator teres force is the highest among all components and is greater in pronation and elbow extension. The radial component becomes negative in pronation and reaches lower values as the elbow flexes. Both components could enhance radial curvature, especially in pronation. The model also enables to calculate efficiency and force components simulating changes in osteometric parameters. An increase of radial curvature improves efficiency and displaces the position where the radial component becomes negative towards the end of pronation. A more proximal location of pronator teres radial entheses and a larger humeral medial epicondyle increase efficiency and displace the position where this component becomes negative towards forearm neutral position, which enhances radial curvature. Efficiency is also affected by medial epicondylar orientation and carrying angle. Moreover, reaching an object and bringing it close to the face in a close-to-neutral position improve efficiency and entail an equilibrium between the forces affecting the elbow joint stability. When the upper-limb skeleton is used in positions of low efficiency, implying unbalanced force components, it undergoes plastic changes, which improve these parameters. These findings are useful for studies on ergonomics and orthopaedics, and the model could also be applied to fossil primates in order to infer their locomotor form. Moreover, activity patterns in human ancient populations could be deduced from parameters reported here.

Citation: Ibáñez-Gimeno P, Galtés I, Jordana X, Malgosa A, Manyosa J (2014) Biomechanics of Forearm Rotation: Force and Efficiency of Pronator Teres. PLoS ONE 9(2): e90319. doi:10.1371/journal.pone.0090319

Editor: David Carrier, University of Utah, United States of America

Received: October 1, 2013; **Accepted:** January 28, 2014; **Published:** February 28, 2014

Copyright: © 2014 Ibáñez-Gimeno et al. This is an open-access article distributed under the terms of the Creative Commons Attribution License, which permits unrestricted use, distribution, and reproduction in any medium, provided the original author and source are credited.

Funding: This work is supported by grants from the Ministerio de Ciencia e Innovación (grant no. CGL2008-00800/BOS), the Generalitat de Catalunya (grant no. 2009 SGR 566), the Programa de Formació de Profesorado Universitario, Ministerio de Educación, Cultura y Deporte (grant no. AP2009-5102) awarded to Pere Ibáñez-Gimeno and the Programa Juan de la Cierva, Ministerio de Economía y Competitividad (grant no. JCI-2010-08157) awarded to Xavier Jordana. The funders had no role in study design, data collection and analysis, decision to publish, or preparation of the manuscript.

Competing Interests: The authors have declared that no competing interests exist.

* E-mail: joan.manyosa@uab.cat

Introduction

The effect of muscular forces on bone structure can be predicted from osteometric parameters using biomechanical models if the line of action and the origins of the tendon are known [1,2]. The rotational efficiency (E_{rot}) of the pronator teres (PT) is a measure of its rotational capacity as a function of the applied force [3]. The PT E_{rot} can be calculated from several osteometric parameters of the upper-limb skeleton, basically related to the curvature of the diaphysis of the radius bone, the size and shape of the humeral medial epicondyle, and the proximo-distal location of PT radial entheses [3–5].

During resisted pronation, PT acts as the primary agonist, displaying relatively higher activity levels than pronator quadratus [6]. In contrast to the latter, PT is largely affected by elbow and forearm position [6,7]. The positioning of the forearm may also influence the components of PT force, which in turn can entail structural changes with different functional implications. There-

fore, it can be hypothesized that each component influences the skeletal structure in a different way, e.g. a component may enhance the curvature of the radius when it exerts a bending loading on its shaft [3]. However, the biomechanical behavior and structural effects of these components in the pronation-supination and flexion-extension ranges have never been examined.

This study aims to analyze PT E_{rot} for a full range of elbow flexion angles in order to (i) analyze the relationship between the components of the force vector and the skeletal structure, (ii) assess how E_{rot} is modified by changes in several osteometric parameters and (iii) get further knowledge about the functional implications of the variation of this parameter in the flexion-extension range. The results of this biomechanical analysis will lay the foundations for future studies about comparative and evolutionary anatomy, as well as works on applied sciences, such as ergonomics, sports medicine and orthopaedics, providing relevant information about

the relationship between the skeletal structure and PT functionality.

Materials and Methods

Materials

The skeletal remains used in this study are part of an osteological collection housed at Unitat d'Antropologia Biològica (Universitat Autònoma de Barcelona). The skeletons in this collection were ceded to Unitat d'Antropologia Biològica (Universitat Autònoma de Barcelona) by Cementiri de Granollers (Ajuntament de Granollers). This session was subjected to prior agreement between both institutions. Moreover, this study is part of a project (CGL2008-00800/BOS), which was approved by Ministerio de Ciencia e Innovación (Gobierno de España).

Rotational efficiency was calculated for the right upper-limb skeleton (humerus, radius and ulna) of a 32-year-old male from the abovementioned collection. The E_{rot} of the studied individual was previously shown to be within to the human pattern of variation, calculated for full elbow extension (180°) and intermediate flexion (90°) [5]. The biomechanical model used in the current study enables to calculate E_{rot} as function of the elbow flexion angle by using 3D imaging techniques. NextEngine's 3D Scanner was used to obtain a three-dimensional image of the humerus, which was processed with ScanStudio HD software [8]. The image was exported to the modeling software Rhinoceros 4.0 SR1 [9], where planes and axes were defined and measurements were taken.

Calculation of pronator teres rotational efficiency

Galtés et al. [3] developed the biomechanical model to calculate the rotational efficiency (E_{rot}) of the pronator teres (PT), which was initially based on the use of CT scan images of the upper-limb. In accordance with this work, E_{rot} is defined by the expression:

$$E_{rot} = \cos \alpha \times \cos \beta \times \overline{AO'}$$

The biomechanical model was later adapted to calculate E_{rot} using skeletal remains by means of photographs of the distal epiphysis of humerus [4]. Although this methodology was simple and practical, the technique was limited since the spatial representation of the humeral planes was not possible. Therefore, some assumptions about the arm and forearm mechanics and the representation of the geometrical points used to calculate E_{rot} had to be made. The use of 3D imaging, basically to define the humeral planes and axes and to determine important details of the medial epicondyle, enabled to obtain more accurate calculations of E_{rot} [5]. As a matter of fact, the calculation of E_{rot} at any elbow position described in the current paper is based on the approach developed by Galtés et al. [4] and Ibáñez-Gimeno et al. [5]. In order to calculate angles α and β at a given forearm and elbow position, several parameters are required (Table 1) [5]. Two of these parameters, l_1 distance and $\overline{OB'}$ distance, depend on the value of carrying angle (λ) and thus vary throughout the flexion-extension range (Fig. 1) [10]. The carrying angle is the angle between the arm and the forearm long axes (Fig. 1). Assuming a linear variation of this angle between a maximum value (λ_m) in full elbow extension (180°), which is measured on dry bones [11], and $\lambda = 0^\circ$ in full elbow flexion (40°) [10,12–14], and using \overline{XB} and \overline{XC} values (Fig. 1B) obtained from the three-dimensional image of the humerus, we can obtain:

$$\Delta l_1(\lambda_m) = l_1(180^\circ) - l_1(40^\circ) = \overline{CB} \times \sin(\omega + \lambda) - \overline{CB} \times \sin \omega \quad (\text{Eq.1})$$

$$\Delta \overline{OB'}(\lambda_m) = \overline{OB'}(180^\circ) - \overline{OB'}(40^\circ) = \overline{CB} \times \cos(\omega + \lambda) - \overline{CB} \times \cos \omega \quad (\text{Eq.2})$$

Distance l_1 ($\overline{P_1P_3}$) is the sum of $\overline{P_2P_3}$ and $\overline{P_1P_2}$ (Figs. 1A and 2A). $\overline{P_2P_3}$ can be measured directly on the radius bone (Figs. 1A and 2A, l_{p1}), and $\overline{P_1P_2}$ can be obtained from: (i) geometric parameters obtained from the three-dimensional image of the humerus (R_c , d_e , ε , Fig. 2B); (ii) the position of the humeral medial epicondyle at each flexion angle (Fig. 2B), and (iii) the position of the elbow flexion axis, which depends on the carrying angle (λ) and varies throughout the flexion-extension range (see Fig. 1 and Eq. 1) [10]. Then, the distance l_1 in maximum elbow extension can be calculated as follows:

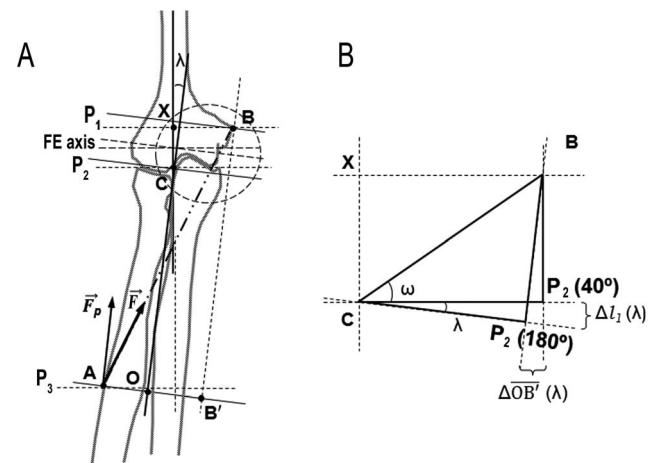


Figure 1. Representation of the influence of carrying angle (λ) on several parameters used to calculate rotational efficiency.

A: Anterior view of right distal arm and forearm bones in supination position. Humeral and forearm axes, the flexion-extension axis (FE axis), as well as the force exerted by pronator teres muscle (\vec{F} , from point A to point B), are represented. \vec{F}_p is the vertical component of pronator teres force. Point A indicates pronator teres distal entheses just at the apex of radial curvature. Point B indicates its proximal attachment site, just at the apex of the medial epicondyle, and point B' is the projection of point B on plane P_3 . Planes P_1 , P_2 and P_3 are parallel to each other and perpendicular to the forearm axis. P_1 passes through point B, P_2 passes through the most proximal point of the radial head and P_3 passes through point A. Point X is the intersection between humeral axis and a plane perpendicular to the humeral axis that passes through point B. Point C is the most distal humeral point of the humeral axis. Point O is the intersection between plane P_3 and the forearm axis. The dashed circle indicates the zoomed-in area of the right image. **B:** Detail of the left image. Plane P_2 is represented for a position of full elbow extension (P_2 (180°)) and for a position of full elbow flexion (P_2 (40°)). The variation of this plane is caused by the variation of the carrying angle (λ). This causes a variation in l_1 and in $\overline{OB'}$ ($\Delta l_1(\lambda)$ and $\Delta \overline{OB'}(\lambda)$), which depends on the elbow angle. Angle ω is the angle between plane P_2 (40°) and \overline{CB} segment.

doi:10.1371/journal.pone.0090319.g001

Table 1. Osteometric and geometric parameters used to calculate forearm rotational efficiency.

| Parameter | Value | Definition |
|-----------------|---------------|--|
| d_r | 1.10 | Radial head radius |
| d_c | 1.10 | Ulnar distal epiphysis radius |
| l_f | 23.00 | Physiological length of the radius |
| l_{pr} | 9.70 | Distance between P_2 and P_3 planes |
| λ_{180} | 10.00° | Carrying angle in full elbow extension |
| ε | 45.65° | Angle between the positive x-axis and the position vector of point B |
| d_e | 0.75 | Distance between flexion-extension axis and point B |
| R_c | 1.14 | Humeral capitulum radius |
| B | (0.52, -0.53) | Coordinates of point B |
| \overline{XB} | 3.93 | Distance between point B and humeral axis |
| \overline{XC} | 1.34 | Distance between P_1 and P_2 planes |
| \overline{AO} | 2.60 | Curvature of the radius |

Distance values are in centimeters. See Materials and Methods and Figures 1, 2 and 3 for further information about the parameters definition. doi:10.1371/journal.pone.0090319.t001

$$l_1(180^\circ) = l_{pr} + R_c + d_e \times \cos\varepsilon + \Delta l_1(\lambda_{180})$$

where $\Delta l_1(\lambda_{180})$ is obtained from Eq. 1. Distance \overline{AO} is the curvature of the radius, measured on dry bone [4,15]. Distance $\overline{OB'}$ (projection of \overline{CB} segment on plane P_3), is dependent on λ value and can be obtained for each position of the elbow using Eq. 2.

Then, $\overline{AO'}$ and $\overline{O'B'}$ can be respectively calculated from \overline{AO} and $\overline{OB'}$ by determining distance $\overline{OO'}$ [4]. Knowing the position of point B and its projection on plane P_3 (Fig. 3), we can calculate, at any flexion angle of the elbow, distance $\overline{AB'}$, angle β , \vec{F}'' and \vec{F}'_r and, therefore, the value of E_{rot} .

Results

Figure 4 shows PT E_{rot} throughout the flexion-extension and the pronation-supination ranges. Rotational efficiency for each elbow position is maximal when the forearm is close to the neutral position (position attained when the thumb points superiorly and the palm faces medially, at 0° of pronation-supination [10]) and is minimal in the extremes of the pronation-supination range. Maximum E_{rot} for each elbow position undergoes a nonlinear growth of 18% from full extension (180°) to full flexion (40°). The position of maximum E_{rot} displaces from -11° of pronation at 180° of elbow extension towards 6° of supination at 40° of elbow flexion (40°) (Fig. 4B). At 120° of elbow flexion, E_{rot} reaches its maximum when the forearm is in the neutral position.

The force that PT exerts on the radius is represented by \vec{F} (Fig. 1). The projection of this vector on the axial plane P_3 is

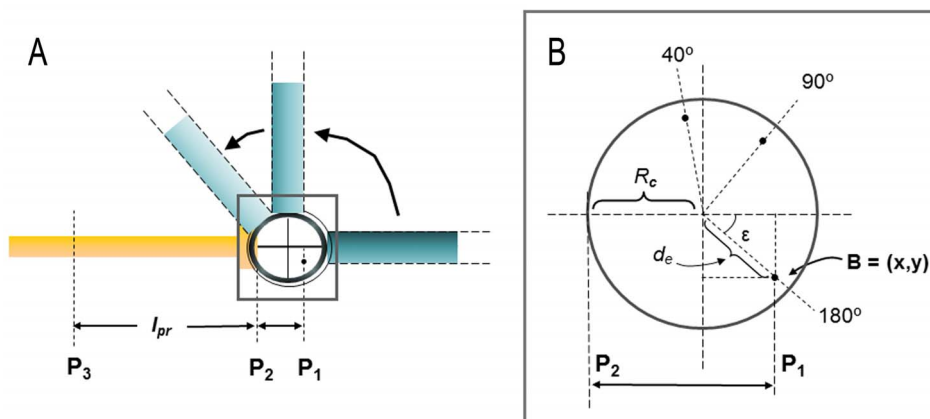


Figure 2. Representation of the changes in position of point B as a function of the elbow angle. **A:** Representation of the elbow in full extension (180°), an intermediate position (90°) and full flexion (40°) from a lateral view. A static radius (yellow) is represented with the humerus in the three positions (blue). Planes P_1 , P_2 and P_3 are represented. The point (point B), and so plane P_1 , are shown for 180° of elbow extension. Distance l_{pr} is the distance between planes P_2 and P_3 . The distance between planes P_1 and P_2 depends on the elbow position. The square indicates the zoomed-in area of the right image. **B:** Change in the position of point B and in the distance P_1P_2 as a function of the elbow angle. The position of point B for the three elbow angles is represented. Point B is positioned in a coordinates system (x, y) which center is the flexion-extension axis from a lateral point of view. R_c is the radius of the humeral condyle. d_e is the distance between the center of coordinates and point B. Angle ε is the angle between the positive x-axis and the position vector of point B. doi:10.1371/journal.pone.0090319.g002

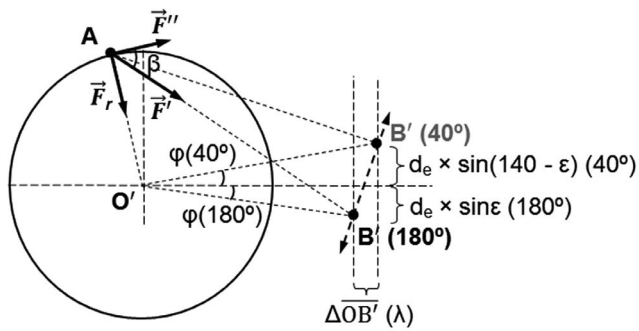


Figure 3. Diagram of plane P_3 with the main parameters to calculate rotational efficiency. Two elbow positions (180° and 40°) are represented. \vec{F}' is the projection of the pronator teres force on plane P_3 . \vec{F}_r is the radial component of \vec{F}' . \vec{F}'' is the component of \vec{F}' tangential to the rotational movement. Angle β is the angle between \vec{F}'' and \vec{F}' . Point A is the radial attachment site of pronator teres. Point O' is the center of the rotational movement. Point B' is the projection of point B on plane P_3 . The position of this point varies as a function of the carrying angle of the elbow ($\Delta\overline{OB'}$ (λ), see Fig. S1) and it is assessed with regards to the horizontal axis by φ angle. The displacement of point B' from the horizontal axis can be calculated from the variation of point B position as a function of the elbow angle (see Fig. 2). doi:10.1371/journal.pone.0090319.g003

represented by \vec{F}' (Fig. 3), whereas the projection on the vertical axis is named \vec{F}_p (Fig. 1). \vec{F}' can be decomposed into two vectors: \vec{F}'' , which is tangent to the trajectory of the radial rotational movement, and \vec{F}_r , which is directed to the rotation center (Fig. 3). Figure 5 shows the relative values for these components at three elbow angles (40° , 90° and 180°). \vec{F}' is greater in supination than in pronation, regardless of the elbow angle. The modulus for the perpendicular component of \vec{F} (F_p) displays values that vary between the 86% and 99% of F value, depending on the pronation-supination and flexion-extension angles. This component increases as the forearm pronates, regardless of the elbow position. It is also slightly greater in extension than in flexion of the elbow.

Concerning the radial component (\vec{F}_r), its modulus values are approximately the 50% of F value in a full supination position for the entire flexion-extension range. These values decrease as the forearm pronates, reaching negatives values in pronation. The forearm position where $F_r = 0$ depends on the elbow angle. At 180° of elbow extension, the modulus for \vec{F}_r reaches 0 at -46° of pronation, whereas in full elbow flexion this occurs at -25° of pronation. Therefore, this component reaches lower negative values, i.e. higher values for its modulus being the vector negative, as the elbow flexes (up to 15% in full flexion). Regarding \vec{F}'' , which modulus does not reach the 40% of F , its values change in a similar way to the values of E_{rot} . The pronation-supination angle where $F'' = F_r$ is dependent on the elbow position. At 180° , it is close to the neutral position of the forearm (at 11° of supination). As the elbow flexes, it displaces towards a more supinated position of the forearm, reaching 31° of supination in full flexion.

Several simulations were carried out to assess how E_{rot} and \vec{F} components are modified by changes in some osteometric parameters. From the mathematic expression to calculate E_{rot} (see Materials and Methods and Figures 1, 2 and 3), it is easily inferable that a greater curvature of the radius (\overline{AO}), and so a greater rotational radius ($\overline{AO'}$), leads to a proportional increase in

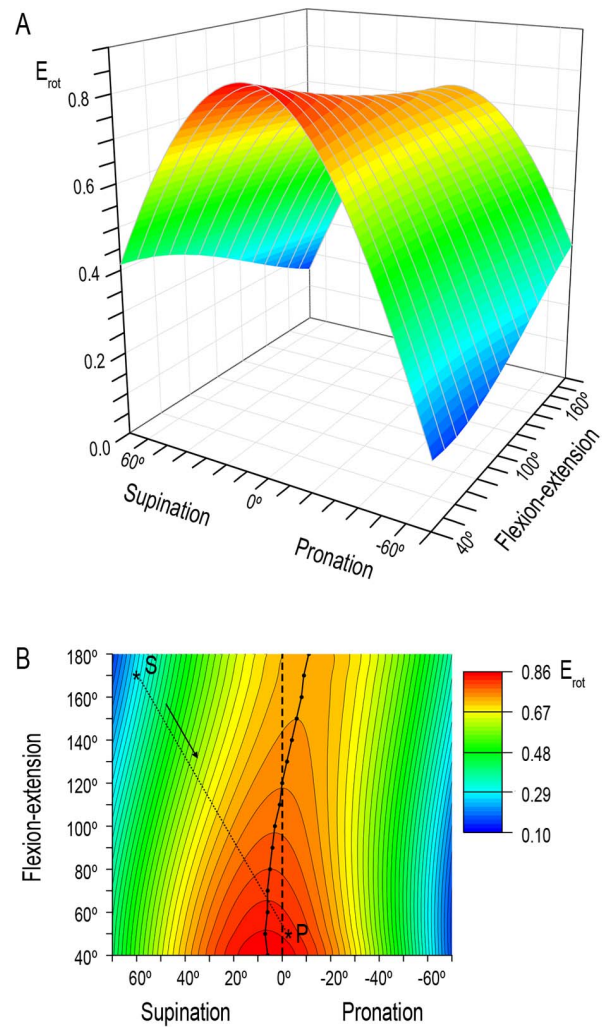


Figure 4. Forearm rotational efficiency (E_{rot}) as a function of pronation-supination and flexion-extension angles. **A:** Three-dimensional surface showing efficiency values at each forearm and elbow angles. **B:** Projection of the three-dimensional surface on XY plane showing efficiency ranges at each forearm and elbow angles. The points connected by a continuous line indicate the forearm positions where efficiency is maximal for each elbow angle. The dashed line indicates the neutral position of the forearm. The dotted line shows a trajectory followed by the forearm to reach an object with the elbow almost fully extended (170°) and the forearm supinated (60°) (asterisk S) and to bring it close to the face (50° of elbow flexion and -5° of pronation) (asterisk P). This trajectory, which direction is indicated by the arrow, is the shortest and entails an increase of about 190% in the efficiency value. doi:10.1371/journal.pone.0090319.g004

the E_{rot} values (Fig. 6A). Moreover, any change in one or several osteometrical parameters that causes an increase of α and/or β angles will consequently enhance E_{rot} (see Materials and Methods). Hence, the moment of force can be improved by rising either the tangential force (\vec{F}'') or the curvature of the radius (\overline{AO}). Although both scenarios would cause an increase in E_{rot} , they are related to different structural characteristics. A 10% rise of \overline{AO} has a minor effect on the components of \vec{F} , being \vec{F}'' modulus constant (Fig. 6A) and slightly reducing \vec{F}_r modulus at -70° of pronation, from 8–15% to 6–13% of F value, depending on elbow position. When a similar increase in E_{rot} is simulated by a 10%

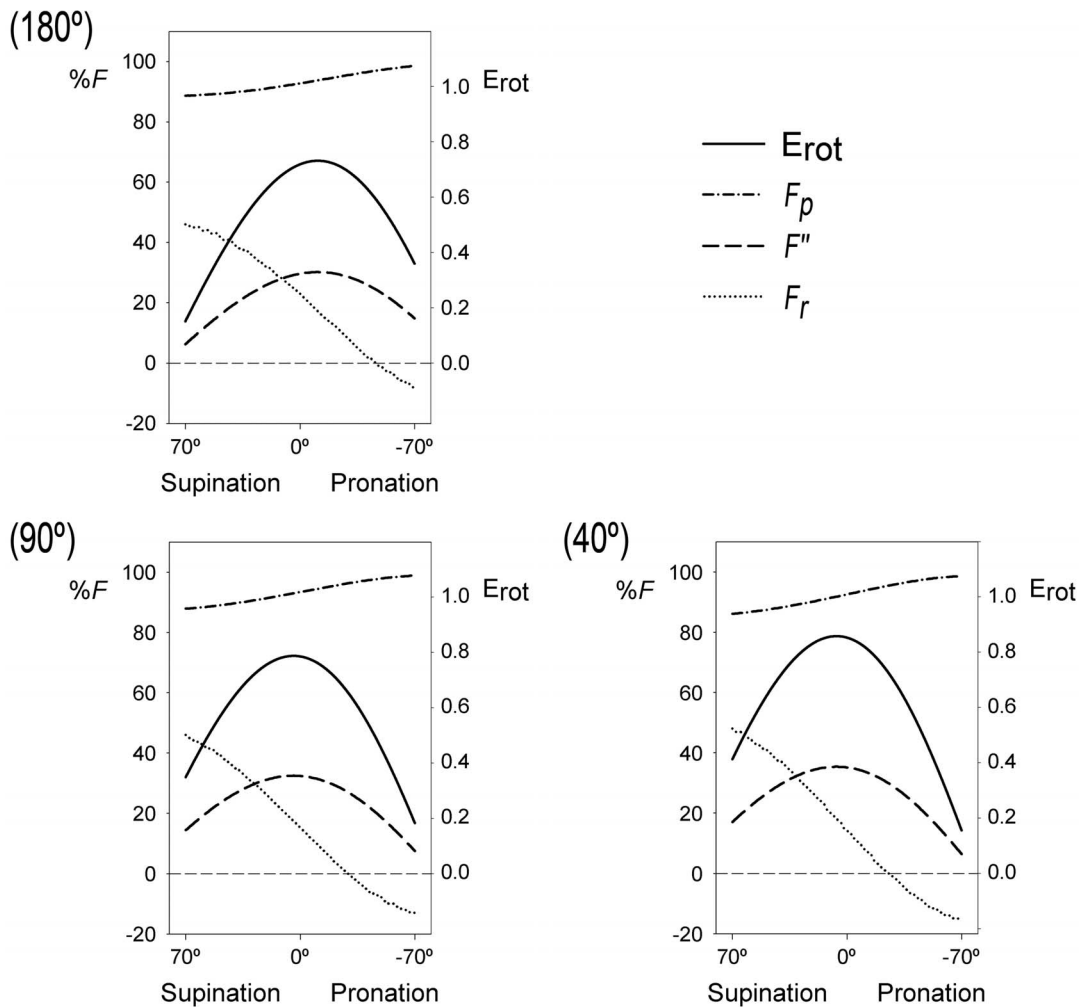


Figure 5. Relative values for \vec{F} components and forearm rotational efficiency (E_{rot}) in three elbow positions. Full extension (180°), intermediate position (90°) and full elbow flexion (40°) scenarios are shown. doi:10.1371/journal.pone.0090319.g005

decrease of l_{pr} , a completely different behavior of \vec{F} vectors can be observed: \vec{F}'' modulus increases proportionally to E_{rot} during the entire flexion range (Fig. 6B), whereas \vec{F}_r modulus rises from 46–48% to 49–51% of F value at 70° of supination and from 8–15% to 10–19% at -70° of pronation. A 10% increase of \overline{XB} has broadly the same effect on E_{rot} and \vec{F}'' and \vec{F}_r moduli than the reported 10% decrease of l_{pr} . \vec{F}_p is not meaningfully modified by changes in the abovementioned parameters, whereas the forearm positions where \vec{F}_r modulus reaches 0, where \vec{F}'' and \vec{F}_r become equal and where E_{rot} is maximal are considerably affected by these changes. All this information is summarized in Table 2.

Conversely to the abovementioned simulations, the direction of the change in E_{rot} and \vec{F}'' modulus (increase or decrease) caused by a change in the position of point B depends on the elbow angle (Fig. 6C). When coordinate x increases, maximal E_{rot} and \vec{F}'' modulus rise in flexion of the elbow and decrease in extension. When this coordinate is lower, the values for these parameters decrease in flexion and rise in extension. When coordinate y is closer to 0, E_{rot} and \vec{F}'' modulus increase in flexion and fall in

extension, whereas when this coordinate is lower, these parameters decrease in flexion and rise in extension.

Efficiency is also lower when the carrying angle (λ) is greater. A change of 5° in this angle leads to a variation of about 6.5% of the maximum E_{rot} value at 180° of elbow extension. This effect is lesser as the elbow flexes and it is null in full flexion (40°).

Discussion

Rotational efficiency, force components and structural implications

In the current study, PT E_{rot} has been assessed throughout the entire flexion-extension range using three-dimensional technology. The variation of E_{rot} obtained from our innovative biomechanical model is in agreement with the results of kinematic studies using cadaveric specimens [16,17] and virtual and resin models of the upper-limb skeleton [18–20], as well as with analysis on forearm discomfort [21] and on electromyographic signals of the forearm pronators [7].

Pronator teres E_{rot} is dependent on the skeletal structure of the arm, elbow and forearm, which in turn can be modified by the usage of this muscle. In this regard, the analysis of E_{rot} has enabled to study the effect of the components of PT force vector on the

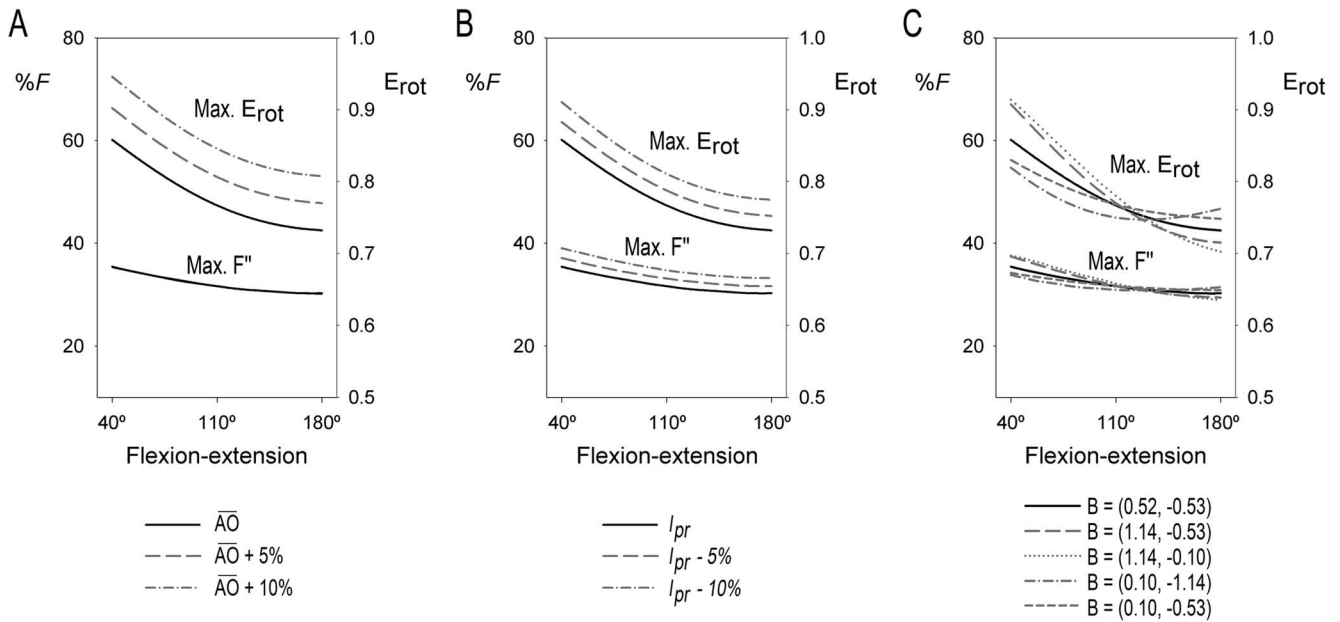


Figure 6. Simulated changes on maximum rotational efficiency (Max. E_{rot}) and maximum F'' value (Max. F''). Simulations are shown throughout the flexion-extension range. **A:** Simulations of an increase in \overline{AO} . Note that the relative values for F'' of the three simulations overlap. **B:** Simulations of a decrease in l_{pr} . The effect caused by an increase in \overline{XB} is similar to the effect caused by the decrease in l_{pr} shown here. **C:** Simulations with different coordinates of point B (cm). doi:10.1371/journal.pone.0090319.g006

upper-limb skeleton. The perpendicular component of this vector (\vec{F}_p) shows high relative values, which indicates that an important part of PT force is employed in a direction parallel to the rotational axis of the forearm, i.e. compressing the radius lengthwise towards the distal epiphysis of the humerus. This compression is also produced during the contraction of other upper-limb muscles, such as biceps brachii and the wrist and fingers flexors. As regards PT, the compressive effect on the radius is higher in pronation than in supination and slightly decreases from elbow extension to maximum flexion. Although the differences are slight, this indicates that pronated positions of the forearm enhance the curvature of the radius through radial compression in a greater degree than supinated positions. This effect is independent of the skeletal structure, as \vec{F}_p is broadly unaffected by changes in the parameters used to calculate E_{rot} .

When the forearm is pronated, biceps brachii is reflexly inhibited and plays little if any role in flexion, because it would supinate the forearm during contraction [22–24]. As mentioned, the perpendicular component of PT force is greater on the prone forearm. This increase may partially compensate the lack of action

of biceps brachii, enhancing the assisting role of PT as elbow flexor and joint stabilizer in this position.

The component \vec{F}_r , which directs to the rotation center, reaches negative values in forearm pronation. When this component is negative, the vector directs opposite to the rotational center, and so it enhances the curvature of the radius. Negative values are reached in a position of the forearm that gets closer to the neutral position as the elbow flexes. Therefore, the curvature of the radius (\overline{AO}) is enhanced during pronation in flexion rather than in extension of the elbow. In any case, the relative values for \vec{F}_r responsible for the curvature of the radius are low when compared to values for \vec{F}_p , which suggests that radii with marked curvatures are more probably associated to compression forces from PT, among other muscles, than to forces applied perpendicularly to the forearm axis. These findings are in agreement with a previous empirical study that revealed that the pattern of muscular loading exerted on the apex of the radial shaft curvature by the PT muscle plays an important role as a mechanical stimulus involved in diaphyseal bowing [15].

Table 2. Effect of the simulations on \vec{F} components and rotational efficiency (E_{rot}) for three elbow positions (180°, 90° and 40°).

| Simulation | Forearm position where $F_r=0$ | | | Forearm position where $F'' = F_r$ | | | Forearm position where E_{rot} is maximal | | |
|---------------------------------|--------------------------------|------|------|------------------------------------|-----|-----|---|-----|-----|
| | 180° | 90° | 40° | 180° | 90° | 40° | 180° | 90° | 40° |
| Original values | -47° | -29° | -25° | 11° | 28° | 31° | -11° | 4° | 6° |
| \overline{AO} increase (+10%) | -52° | -34° | -30° | 8° | 25° | 28° | -11° | 4° | 6° |
| l_{pr} decrease (-10%) | -44° | -27° | -23° | 13° | 29° | 34° | -11° | 3° | 5° |
| \overline{XB} increase (+10%) | -42° | -26° | -23° | 14° | 29° | 33° | -10° | 3° | 5° |

doi:10.1371/journal.pone.0090319.t002

The effect that the skeletal structure and form have on E_{rot} and on the force vectors has also been assessed. The results show that a greater bowing of the radius entails an increase of E_{rot} . This is consistent with previous studies suggesting an enhancement of PT action and forearm rotational power by a markedly bowed radius [3,25–28]. An increase of the radial curvature also causes that \vec{F}_r becomes negative in a more pronated position of the forearm, and so its modulus reach lower values in full pronation. Therefore, the radius is more easily bowed when its curvature is low.

The radial location of PT muscle also affects E_{rot} : at any elbow angle, E_{rot} increases when this enthesis is more proximally located, which is consistent with previous observations in full elbow extension [3]. Moreover, radii with a more proximal enthesis for PT muscle lead to the reach of negative values of \vec{F}_r closer to the neutral position of the forearm. Therefore, these radii entail lower negative values for this component, i.e. higher values for its modulus being the vector negative, which stimulates radial curvature.

Concerning the humeral medial epicondyle, E_{rot} also tends to increase in all elbow positions as this structure enlarges. Even though the current analysis uses a different approach to quantify humeral medial epicondylar projection (\overline{XB}), the results are consistent with previous studies [3,5,29]. Moreover, an enlargement of the medial epicondyle has the same effect on \vec{F}_r than a more proximally located radial enthesis for PT, and therefore a more medially projected epicondyle enhances radial curvature.

The orientation of the medial epicondyle is also relevant for the determination of E_{rot} . The alteration of this orientation causes changes in \vec{F}'' that lead to changes in E_{rot} . A more posteriorly oriented epicondyle, i.e. more retroflexed [5,30], is associated with a greater E_{rot} in full extension of the elbow, whereas an epicondyle with a lower degree of retroflexion has greater values of E_{rot} in full flexion. Moreover, a more proximally oriented epicondyle enhances E_{rot} in full flexion, whereas when it is more distally oriented, E_{rot} increases in extension. The orientation of the medial epicondyle was reported to present a partially activity-dependent plasticity, and so it was hypothesized that it can be modified to enhance certain abilities [30]. In this regard, and in agreement with the abovementioned relationship between E_{rot} and epicondylar orientation, a simple observation of the upper-limb positioning shows that a habitual and continued contraction of PT in full elbow flexion would reorient the epicondyle towards a more proximal position. Conversely, this reorientation would occur distally in full elbow extension. The reported association between the orientation of the medial epicondyle and E_{rot} may have important implications on the evolutionary pathway of the upper-limb skeleton, as this structure plays a central role in the locomotor diversity of primates [5,31–33].

Regarding the carrying angle of the elbow [11], this is the first quantitative insight into its biomechanical implications on forearm rotation. An increase in this angle leads to lower values of E_{rot} . This effect is the greatest in full elbow extension and becomes lower as it is flexed, given that carrying angle is maximal in full extension, decreases during flexion and reaches 0° when the elbow is completely flexed [10,12–14].

Functional implications of forearm rotation

The biomechanical model described here enables to make a thorough quantitative approach to clarify some mechanical aspects about the relationship between PT and forearm and elbow motion. For instance, the results indicate that maximal E_{rot} for each elbow angle is close to the neutral position of the forearm. This position has been commonly associated to the functional

position, which minimizes the expenditure of muscular energy as it implies a natural equilibrium between antagonist muscles [10]. Moreover, it entails an enhancement of the precision of the grip, because the forearm axis is in line with the pronation-supination axis [10,34].

Although skeletal structures with different morphologies can have the same E_{rot} , they do not have to imply the same abilities in terms of precision. For instance, if the same force is exerted by PT on two upper-limbs with the same E_{rot} , the one with the greatest curvature will be able to reach a lower rotational angle (File S1 and Fig. S1), and thus a greater rotational precision.

The stability of the elbow joint has relevant implications for sports medicine and other pathological conditions [14,35,36]. During pronation, \vec{F}' plays an important role in the stability of the radio-ulnar joint (see File S1 and Fig. 3), whereas \vec{F}_p participates in the radio-humeral stability (see Fig. 1A). The global stability of the elbow is thus enhanced by the combination of both components. Although \vec{F}_p is slightly lower when the forearm is supinated, the great \vec{F}' value in this position leads to a better fitting between the radius and the ulna than in pronation [37].

Rotational efficiency and the forces that act during pronation may be associated to the estimations of the discomfort levels done by Mukhopadhyay et al. [38], as the movements implying a high level of discomfort correspond to positions where E_{rot} is low. Moreover, the concept “efficiency” provides information about the rotational stability of a given position, as the work needed to modify the forearm rotational angle depends directly on the value of E_{rot} in each position (see File S1). For a given pronation movement, the model can be used to determine the trajectories of the hand that entail the minimal expenditure of energy for PT. In humans, pronation is usually performed when an object has been reached with the hand supinated and the elbow extended and is then brought closer to the body. The final position of this movement will entail a full flexion of the elbow and a close-to-neutral position of the forearm. This movement implies an increase of PT E_{rot} , which indicates that the energy expenditure of this muscle diminishes when the elbow is flexed (see Fig. 4B). The results show that a great part of this trajectory entails upper-limb positions where \vec{F}'' and \vec{F}_r have a similar value, i.e. around the forearm position where $F'' = F_r$. This indicates that during this trajectory the forces that the elbow joint is submitted to are quite equilibrated.

These two conditions (equilibrium between forces and increase of E_{rot}) are not observed for other trajectories, such as those where the end point is close to full pronation with the elbow flexed. In this case, the final part of the trajectory entails a decrease of E_{rot} and very different values of these two force components. If the forearm was very regularly used to perform this movement with important mechanical loads, the disequilibrium could have pathological consequences, as a result of heavy tensions in the radio-ulnar proximal joint. In order to minimize the expenditure of energy and to rebalance the forces, the radial curvature could increase. As reported by our simulations, a rise of the curvature of the radius causes an increase of E_{rot} and a displacement of the position where $F_r=0$ towards full pronation, as well as a displacement of the position where \vec{F}_r and \vec{F}'' become equal from supination towards a position closer to the neutral.

Therefore, the results of the current study also indicate that the upper-limb skeleton may experience plastic changes as a result of PT activity when it is used in positions where E_{rot} is low and forces are not equilibrated. These changes entail an improvement of these parameters, in order to adjust to the unfavorable conditions.

Conversely, if the upper-limb is mainly used in positions with high E_{rot} values, PT will not trigger changes in the skeletal structure. Overall, E_{rot} and its relationship with energy expenditure and rotational stability, as well as the relative values of the force components, which are linked to the joint stability, provide a global insight into pronation and its association to the forearm skeletal structure. These findings will be useful for future analyses on ergonomics and orthopaedics of the upper-limb skeleton, as they provide relevant information about the relationship between PT functionality and the skeletal structure.

Applying this biomechanical model on studies about comparative anatomy of primate taxa would provide valuable information about the functional meaning of the upper-limb skeletal interspecific differences, which will probably be associated to the locomotor abilities of each taxon. Moreover, an analysis of PT E_{rot} and force components on a fossil primate would very useful for inferring its upper-limb involvement in locomotion.

Some skeletal parameters essential for the determination of PT functionality, such as the radial curvature and the medial epicondylar form, are reported to be plastic and related to the usage of PT muscle [15,30]. Therefore, this biomechanical model would also be of great interest if applied to ancient human populations. Differences in parameters derived or related to E_{rot} between sexes, groups or populations would account for differences in occupational and habitual activities.

Supporting Information

Figure S1 Diagrams showing the displacement caused by a force in different scenarios. A: Linear displacement (Δs)

References

- Murray WM, Buchanan TS, Delp SL (2002) Scaling of peak moment arms of elbow muscles with upper extremity bone dimensions. *J Biomech* 35: 19–26.
- Tsaopoulos DE, Maganaris CN, Baltzopoulos V (2007) Can the patellar tendon moment arm be predicted from anthropometric measurements? *J Biomech* 40: 645–651.
- Galtés I, Jordana X, Cos M, Malgosa A, Manyosa J (2008) Biomechanical model of pronation efficiency: New insight into skeletal adaptation of the hominoid upper limb. *Am J Phys Anthropol* 135: 293–300.
- Galtés I, Jordana X, Malgosa A, Manyosa J (2009) Technical note: Forearm pronation efficiency analysis in skeletal remains. *Am J Phys Anthropol* 140: 589–594.
- Ibáñez-Gimeno P, Jordana X, Manyosa J, Malgosa A, Galtés I (2012) 3D analysis of the forearm rotational efficiency variation in humans. *Anat Rec* 295: 1092–1100.
- Gordon KD, Pardo RD, Johnson JA, King GJW, Miller TA (2004) Electromyographic activity and strength during maximum isometric pronation and supination efforts in healthy adults. *J Orthop Res* 22: 208–213.
- O'Sullivan LW, Gallwey TJ (2002) Upper-limb surface electro-myography at maximum supination and pronation torques: the effect of elbow and forearm angle. *J Electromyogr Kines* 12: 275–285.
- ScanStudio HD 1.2.1 (2006) Software for Windows. Santa Monica: NextEngine, Inc.
- Rhinoceros 4.0 SR1 (2007) Educational Edition for Windows. Seattle: Robert McNeel & Associates.
- Kapandji AI (2002) *Fisiología articular, miembro superior*. Madrid: Editorial Médica Panamericana.
- Knussmann R (1967) Humerus, ulna und radius der Simiae. *Bibl Primatol* 5: 1–399.
- Morrey BF, Chao EYS (1976) Passive motion of the elbow joint. *J Bone Joint Surg Am* 58: 501–508.
- Rouvière H, Delmas A (1988) *Anatomía humana: Descriptiva, topográfica y funcional*, tomo III, 9th ed. Barcelona: Masson.
- Goto A, Moritomo H, Murase T, Oka K, Sugamoto K, et al. (2004) In vivo elbow biomechanical analysis during flexion: Threedimensional motion analysis using magnetic resonance imaging. *J Shoulder Elbow Surg* 13: 441–447.
- Galtés I, Jordana X, Manyosa J, Malgosa A (2009) Functional implications of radial diaphyseal curvature. *Am J Phys Anthropol* 138: 286–292.
- Murray WM, Delp SL, Buchanan TS (1995) Variation of muscle moment arms with elbow and forearm position. *J Biomech* 28: 513–525.
- Haugstvedt JR, Berger RA, Berglund LJ (2001) A mechanical study of the moment-forces of the supinators and pronators of the forearm. *Acta Orthop Scand* 72: 629–634.
- Lan N, Baker L (2004) Biomechanical couplings between elbow and forearm movements. *Conf Proc IEEE Eng Med Biol Soc* 6: 4661–4664.
- Bremer AK, Sennwald GR, Favre P, Jacob HAC (2006) Moment arms of forearm rotators. *Clin Biomech* 21: 683–691.
- Hale R, Dorman D, Gonzalez RV (2011) Individual muscle force parameters and fiber operating ranges for elbow flexion-extension and forearm pronation-supination. *J Biomech* 44: 650–656.
- O'Sullivan LW, Gallwey TJ (2001) Forearm discomfort for repeated isometric torque exertions in pronation and supination. In: Hanson MA, editor. *Contemporary ergonomics 2001*. London: Taylor and Francis. pp. 79–83.
- Basmajian JV, Latif A (1957) Integrated actions and functions of the chief flexors of the elbow: A detailed electromyographic analysis. *J Bone Joint Surg Am* 39-A: 1106–1118.
- Naito A, Shimizu Y, Handa Y, Ichie M, Hoshimiya N (1991) Functional anatomical studies of the elbow movements I: Electromyographic (EMG) analysis. *Okajimas Folia Anat Jpn* 68: 283–288.
- Latarjet M, Ruiz Liard A, Pró E (2004) *Anatomía humana*. Buenos Aires: Médica Panamericana.
- Trinkaus E, Churchill SE (1988) Neandertal radial tuberosity orientation. *Am J Phys Anthropol* 75: 15–21.
- Aiello L, Dean C (1990) *An introduction to human evolutionary anatomy*. London: Academic Press.
- Tuttle RH, Hollowed JR, Basmajian JV (1992) Electromyography of pronators and supinators in great Apes. *Am J Phys Anthropol* 87: 215–226.
- Rose MD (1993). Functional anatomy of the elbow and forearm in primates. In: Gebo DL, editor. *Postcranial adaptation in nonhuman primates*. DeKalb: Northern Illinois University Press. pp. 70–95.
- Jablonski NG, Leakey MG, Kiarie C, Antón M (2002) A new skeleton of *Theropithecus brumpti* (Primates: Cercopithecidae) from Lomekwi, West Turkana, Kenya. *J Hum Evol* 43: 887–923.
- Ibáñez-Gimeno P, Galtés I, Jordana X, Fiorin E, Manyosa J, et al. (2013) Enteseal changes and functional implications of the humeral medial epicondyle. *Int J Osteoarchaeol* 23: 211–220.
- Seiffert ER, Simons EL, Fleagle JG (2000) Anthropoid humeri from the late Eocene of Egypt. *Proc Natl Acad Sci* 97: 10062–10067.
- Ciochon RL, Gunnell GF (2004) Eocene large-bodied primates of Myanmar and Thailand: Morphological considerations and phylogenetic affinities. In: Ross CF, Kay RF, editors. *Anthropoid origins: New visions*. New York: Kluwer Academic/Plenum Publishers. pp. 249–282.
- MacPhee R, Meldrum J (2006) Postcranial remains of the extinct monkeys of the Greater Antilles, with evidence for semiterrestriality in *Paralouatta*. *Am Mus Novit* 3516: 3–65.

and rotational angle ($\Delta\theta$) caused by a force \vec{F} on a rotating body, being the center of rotation O and the rotational radius R. **B:** Representation of the differences in the force (\vec{F}_1 and \vec{F}_2) that are needed to obtain the same rotational angle when the rotation performed by pronator teres muscle starts at a different point (A_1 and A_2) (see Fig. 3). **C:** Representation of the differences in the rotational angle ($\Delta\theta_1$ and $\Delta\theta_2$) obtained when the same force (\vec{F}) is applied by pronator teres muscle on two radii with different rotational radius (r_1 and r_2) (see Fig. 3). Note that the same linear displacement (Δs) is obtained in both cases.

(TIF)

File S1 Rotating work during forearm pronation, stability and muscular energy expenditure.

(DOCX)

Acknowledgments

The authors are grateful to Antoni Morros for his assistance in the preparation of the artwork. They are also indebted to the Academic Editor, David Carrier, and an anonymous reviewer for their comments on an earlier version of the manuscript.

Author Contributions

Conceived and designed the experiments: PI IG JM. Performed the experiments: PI JM. Analyzed the data: PI IG XJ AM JM. Contributed reagents/materials/analysis tools: XJ AM. Wrote the paper: PI JM. Revised the paper: PI IG XJ AM JM.

34. Marzke MW (1997) Precision grips, hand morphology, and tools. *Am J Phys Anthropol* 102: 91–110.
35. Shiba R, Sorbie C, Siu DW, Bryant JT, Cooke TDV, et al. (1988) Geometry of the humeroulnar joint. *J Orthop Res* 6: 897–906.
36. Richards RR (1996) Chronic disorders of the forearm. *J Bone Joint Surg Am* 78: 916–930.
37. Morrey BF, An KN, Stormont TJ (1988) Force transmission through the radial head. *J Bone Joint Surg Am* 70: 250–256.
38. Mukhopadhyay P, O'Sullivan L, Galloway TJ (2007) Estimating upper limb discomfort level due to intermittent isometric pronation torque with various combinations of elbow angles, forearm rotation angles, force and frequency with upper arm at 90° abduction. *Int J Ind Ergonom* 37: 313–325.